Rock and Soil Mechanics

Volume 41 | Issue 6 Article 6

11-11-2020

# Experimental study on evolution characteristics of water and mud inrush in fault fractured zones

Qing-yan ZHANG
*University of Chinese Academy of Sciences, Beijing 100049, China*

Wei-zhong CHEN
*Geotechnical and Structural Engineering Research Center, Shandong University, Jinan, Shandong 250061, China*

Jing-qiang YUAN
*State Key Laboratory of Geomechanics and Geotechnical Engineering, Institute of Rock and Soil Mechanics, Chinese Academy of Sciences, Wuhan, Hubei 430071, China*, zhangqingyan1990@126.com

LIU-Qi LIU-Qi
*University of Chinese Academy of Sciences, Beijing 100049, China*

*See next page for additional authors*

Follow this and additional works at: https://rocksoilmech.researchcommons.org/journal

 Part of the Geotechnical Engineering Commons

## Custom Citation

ZHANG Qing-yan, CHEN Wei-zhong, YUAN Jing-qiang, LIU-Qi, RONG Chi, . Experimental study on evolution characteristics of water and mud inrush in fault fractured zones[J]. Rock and Soil Mechanics, 2020, 41(6): 1911-1922.

This Article is brought to you for free and open access by Rock and Soil Mechanics. It has been accepted for inclusion in Rock and Soil Mechanics by an authorized editor of Rock and Soil Mechanics.

# Experimental study on evolution characteristics of water and mud inrush in fault fractured zones


## Authors

Qing-yan ZHANG, Wei-zhong CHEN, Jing-qiang YUAN, LIU-Qi LIU-Qi, and Chi RONG



This article is available in Rock and Soil Mechanics: https://rocksoilmech.researchcommons.org/journal/vol41/iss6/6

Rock and Soil Mechanics 2020 41(6): 1911−1922 ISSN 1000−7598
https: //doi.org/10.16285/j.rsm.2019.6527 rocksoilmech.researchcommons.org/journal

# Experimental study on evolution characteristics of water and mud inrush in fault fractured zones

ZHANG Qing-yan[1, 2], CHEN Wei-zhong[1, 3], YUAN Jing-qiang[1], LIU-Qi[1, 2], RONG Chi[1, 2]

1. State Key Laboratory of Geomechanics and Geotechnical Engineering, Institute of Rock and Soil Mechanics, Chinese Academy of Sciences, Wuhan, Hubei 430071, China

2. University of Chinese Academy of Sciences, Beijing 100049, China

3. Geotechnical and Structural Engineering Research Center, Shandong University, Jinan, Shandong 250061, China

**Abstract**: To investigate the mechanism of water and mud inrush in water-rich fault fracture zones, a large-scale indoor water and mud inrush test system considering mass transfer and geostress state is developed. The simulation test of water and mud inrush disasters evolution process in the fault fracture zone with different hydraulic loading modes and medium parameters of fracture zones are carried out using the device. Some findings are as follows: 1) Evolution of water and mud inrush disasters in fault fractured zones is a strong coupling process of seepage and erosion. In the beginning, fine particles in the filling of fracture zones will migrate under the water pressure. Then, with the continuous migration and loss of fine particles, the flow pattern changes from laminar flow to turbulent flow, which eventually leads to water and mud inrush disasters. 2) The larger initial porosity of the filling in the fractured zone and the higher applied water pressure will induce the water inrush more easily. As a result, the evolution characteristics of seepage exhibit more obvious in the test and the increase of seepage field parameters such as permeability, porosity, and Reynolds number is much faster. Therefore, evolution curves of the seepage field parameters suddenly increase. 3) The evolution characteristics of water and mud inrush are more obvious under the gradient loading than under a loading condition with constant water pressure, and the critical water pressure of water and mud inrush from the filling is smaller. A generalized model of permeability evolution characteristics of the fault is established with analysis of flow state transition based on the relationship between water flow rate and time ($Q$−$t$), the relationship between hydraulic gradient and water flow rate ($i$−$Q$), and the relationship between permeability and hydraulic gradient ($k$−$i$) that describes the evolution characteristics of permeability. The results provide guidance for evolution mechanisms and prevention measures of water and mud inrush disasters in fault fractured zones.

**Keywords:** fault fracture zone; experimental study; water and mud inrush; characteristics of seepage evolution

## 1 Introduction

The rock mass in fault fracture zones is incompact, fractured and of low intactness. In the underground engineering, when a tunnel passes through water-rich fault fracture zones, the groundwater and construction disturbance can result in disintegration of the rock mass in fault fracture zones, which further leads to the formation of a water channel. Additionally, water and mud inrush caused by improper disposal makes great damage to human life and property. Therefore, the prevention for water and mud inrush disasters has been a hot and difficult topic in the current underground engineering research[1]. By summarizing a large number of accident cases of water and mud inrush in fault fracture zones at home and abroad[2−10], it is found that high osmotic pressure, excavation disturbance and weak permeability resistance ability of surrounding rocks are the three main factors which result in water and mud inrush disasters of fault fracture zones.

Scholars have carried out the research on the mechanism of water and mud inrush by in-situ and laboratory experiments, theoretical analysis and numerical simulation. They have obtained rich theoretical knowledge and engineering experience, which effectively guide the scientific prediction and prevention of water and mud inrush in underground engineering constructions. Li et al.[11] proposed that the fault zone would become the "barrier" for the deformation and stress propagation of underground space excavation, resulting in the strong accumulation of stress and strain between the fault zone and excavated space. The induced excavation space and large deformation in the fault zone could also lead to the generation of tensile cracks and the infiltration of groundwater. Wu et al.[12] elaborated the weakening mechanism and key factors of hysteretic water inrush, and proposed the weakening effect of water inrush time on the fault structure in coal floor. Shi et al.[13] studied the relationship between the fault location, elements of goaf and water inrush from the perspective of mine pressure, and believed

Received: 4 September 2019 Revised: 25 November 2019
This work was supported by the Research Project on Innovation Groups in Hubei Province (2018CFA012) and the General Program of National Natural Science Foundation of China (51879258).
First author: ZHANG Qing-yan, male, born in 1990, PhD candidate, specializing in the disaster of tunnel water and mud inrush. E-mail: zhangqingyan1990@126.com
Corresponding author: YUAN Jing-qiang, male, born in 1985, PhD, Research assistant, specializing in the disaster of tunnel water and mud inrush, and implementing mechanism. Email: jqyuan@whrsm.ac.cn

that water inrush is likely to occur when the fault plane inclines to the boundary of goaf. Jeon et al.[14] made use of model tests to study the influence of fault, weak surface, and grouting on the stability of tunnel surrounding rock, and found that the deformation and shearing stress of the tunnel surrounding rock significantly increased at the location where the fault and weak surface existed. Ma et al.[15] studied the migration rule of fine particles in granular sandstone samples with different initial porosities, particle gradations and seepage pressures through experiments, and the research results showed that the migration of fine particles played a crucial role in increasing the permeability and porosity of the samples in the process of water inrush. Li et al.[16] investigated the seepage, mechanical properties, and failure mechanisms of the filling medium under the condition of occurrence by a large scale triaxial stress-percolation coupling test system. Li et al.[17] revealed the essential reasons of water inrush in fault fracture zones: excavation disturbance caused the failure of mechanical and seepage balance, which then contributed to the redistribution of stress state of surrounding rock and the release of groundwater energy. Yao[18] considered the variable mass seepage behaviors of the fractured rock in the process of water inrush from coal floor of collapse column, analyzed the influencing factors of mass loss rate of the fractured rock in the process of seepage, and obtained the time-history curves of mass loss rate, porosity and permeability with different particle sizes, stresses and sediment concentrations. Wang et al.[19] used the variable fractured rock mass seepage testing system to test the non-Darcy seepage characteristics of the fractured rock mass, and analyzed the time-varying laws of mass loss rate, porosity, permeability and other parameters during the seepage process of the fractured mudstone. Zhang[20] designed the experimental device to model water and mud inrush in fault zones, and studied the starting migration, mutation, and stable evolution rules of particles in the water inrush process under the conditions with different water pressures, different fault widths and different medium compositions. Chang et al.[21] studied the mechanism of erosion instability inside the dam body. By regulating the external stress of the sample to simulate the law of particle erosion inside the sample under different stress states, they obtained the critical hydraulic gradient of the seepage instability evolution process of the dam body.

Water and mud inrush in tunnel excavation through fault fracture zones is affected by high osmotic pressure and impermeability of the rupture zone. Under the joint action of high osmotic pressure and impermeability, there is a process of development and evolution for the particles eroded by dynamic water in the fault zone. As the flow in the medium transforms from laminar flow to turbulent flow, it will eventually induce water and mud inrush disasters. Therefore, the osmotic pressure and the permeability resistance ability of the fault fracture zone are important indicators to judge whether there is a risk of water and mud inrush in the fault fracture zone. There are still some problems existing in the current research, such as the single boundary condition of model tests, the interaction between stress control system and water pressure control, and the mismatching between the pressure loading mode and the gradient water pressure change in the actual water-resistant structure. Therefore, a set of large indoor test system for water and mud inrush, which can consider particle migrations and the in-situ geostress state, was developed in this study. This system was employed to test the evolution characteristics of water and mud inrush in fault fracture zones with different porosities, two loading conditions of constant and gradient water pressures. The variables of test process were discussed systematically. The evolution relationships of water flow rate, particle loss, permeability, porosity and Reynolds number under two hydraulic loading modes were analyzed. Finally, the permeability evolution characteristics of the fault fracture zone under high osmotic pressure were discussed by analyzing the flow pattern transition based on the relationship of water flow rate over time ($Q$−$t$), the relationship of hydraulic gradient to water flow rate ($i$−$Q$) and the permeability evolution law of the permeability with hydraulic gradient ($k$–$i$).

## 2 Experimental scheme

### 2.1 Experimental system

In order to simulate the process of water and mud inrush disasters in the infill materials of the water-rich fracture zone, a large indoor water and mud inrush test system is independently designed as shown in Fig.1, in which the mass migration and the in-situ stress state are considered[22]. The test system mainly consists of three parts: loading system, seepage system and muddy water collection system.

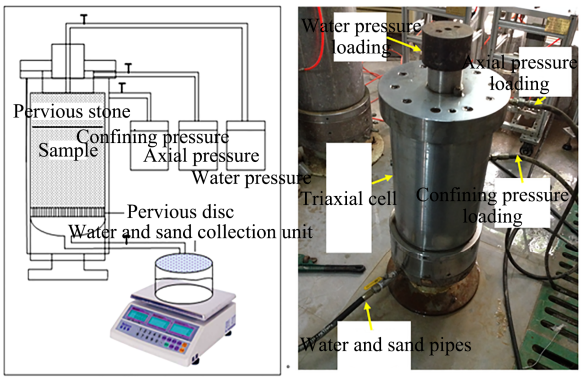


(a) Schematic diagram (b) Real products

**Fig. 1 Experimental system**

(1) Loading system: the loading system is composed

of one gas-driven pressurized pump, three drive converters and three regulators.

(2) Seepage system: the seepage system consists of a triaxial testing cell ($\phi$15 cm×30 cm), a sample barrel, a seepage pipe, and a waterproof board, etc.

(3) Muddy water collection system: it is mainly composed of a funnel, a beaker, a sieve, an oven, and an electronic scale.

### 2.2 Preparation of test materials

The test materials are from the fracture zone of the F1 fault of the YIN-Hong-Ji-Shi Diversion Project in Shaanxi province. The F1 fault has a dip direction of 9º and a dip angle of 64º. The angle between the fault and the axis of the diversion tunnel is about 22º. During the tunnel excavation, the width of the fault was revealed to be 70 meters and there were more than 300 branches and secondary faults in the region. Large mud and water inrush occurred seven times, which caused serious economic and property losses and delayed the construction up to 3 years. The lithology of fault F1 fractured zone is composed of the fractured rock and mylonite with weak cementation and fractured structure, and filled with mud and cuttings.

The particle gradation analysis was carried out for the samples from the fault zone, and the grain grading curve is shown in Fig.2. It is concluded that the rock and soil mass in the fault fracture zone is mainly composed of the rock skeleton and the mixed filling of fine particles according to the grain size distribution curve. Therefore, limestone is chosen as the skeleton for the filling materials of the fault fracture zone in this test. Additionally, the clay fine particles are chosen as the fine particle filling materials. They are both prepared according to the grain size distribution ratio of the F1 fault breccia.

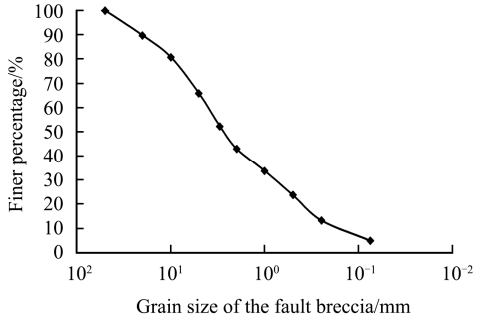


**Fig. 2 Particle size distribution of the fault breccia**

### 2.3 Design of test scheme

In the underground engineering, external water pressure is the power source of water and mud inrush disasters in the fault fracture zones. Therefore, a constant water pressure loading is used to simulate the external water pressure. In addition, as the tunnel is excavated, the palm face is getting closer to the water-rich fault fracture zone and the hydraulic gradient for the water-resistant structure is increasing. In order to investigate the spatial and temporal relationship between the water-resistant structure and the water-rich fault fracture zone after tunnel excavation, the hydraulic loading method with gradient water pressure applied to the filling medium is studied.

In summary, the stress state of the fault is simulated by applying the confining pressure of 0.4 MPa and the axial pressure of 0.5 MPa. Three sets of constant water pressure boundary conditions with 0.4, 0.7 and 1.0 MPa, are applied to simulate the change of external water pressure in the fault fracture zone. At the early stage, 0.02 MPa is a unit pressure gradient for the low water pressure range. When the pressure reaches 0.1 MPa, 0.1 MPa is a unit pressure gradient. Finally, 1 MPa is used as a unit pressure gradient to simulate the dynamic change process of water pressure inside the fault fracture zone caused by the tunnel excavation.

To study the influence of the permeability resistance on the evolution of the filling materials permeability in the fault fracture zone, the initial porosities of the filling materials are 0.35, 0.30 and 0.25 under water pressure in each group. The sample diameter is 150 mm and the height is 200 mm. To make the water pressure evenly distributed, the top of the sample barrel is filled by pervious stones. Table 1 displays the specific experiment scheme.

**Table 1 Experiment scheme**

| Sample No. | Constant water pressure/ MPa | Water pressure gradient / MPa | Initial porosity |
|---|---|---|---|
| 1 | 0.4 | — | 0.25 |
| 2 | 0.7 | — | 0.25 |
| 3 | 1.0 | — | 0.25 |
| 4 | 0.4 | — | 0.30 |
| 5 | 0.7 | — | 0.30 |
| 6 | 1.0 | — | 0.30 |
| 7 | 0.4 | — | 0.35 |
| 8 | 0.7 | — | 0.35 |
| 9 | 1.0 | — | 0.35 |
| 10 | — | 0, 0.02, 0.04, ⋯, 0.1, 0.2, 0.3, ⋯, 1 | 0.25 |
| 11 | — | 0, 0.02, 0.04, ⋯, 0.1, 0.2, 0.3, ⋯, 1 | 0.30 |
| 12 | — | 0, 0.02, 0.04, ⋯, 0.1, 0.2, 0.3, ⋯, 1 | 0.35 |

### 2.4 Test process

(1) Sample preparation. The in-situ geotechnical samples were divided into different particle size ranges, and the particle size distribution curve is shown in Fig.2. Six groups of particle sizes are selected for obtaining the particle ratio of test samples, which are 0−0.075, 0.075−0.5, 0.5−1, 1−3, 3−5 and 5−20 mm, respectively, as shown in Fig.3. Then, according to the weight proportion of the particle size in each group, they were weighed and put into the sample bucket, tamped in layers, and roughened between layers. The contact surface be-

tween the sample and the barrel wall was coated with Vaseline. After adding porous stone, the sample was saturated with water.

(2) Stress boundary application. After the sample was saturated, start the gas-driven pressure pump and drive converter to add specified confining pressure, water pressure and axial pressure on the sample.

**Fig. 3 Test materials for fault fillings**

(3) Evolution test of water and mud inrush. With the constant seepage of pressure water, the rock and soil particles in the fault fracture zone flowed out together with the water flow.

(4) Data collection. Data were collected every 1 min during the test. In the drain pipe, the gauze filter was used to collect the lost particles, and collect and weigh the corresponding gushing water.

(5) Post-test treatment. The device should be cleaned and maintained after the test, and the follow-up tests will be carried out. The experimental data such as water flow rate, particle loss, porosity, permeability and Reynolds number were analyzed, and the law of permeability evolution was discussed.

### 2.5 Test data processing

The particles in the flow were collected every $\Delta t$, and the masses of particles were determined after drying $\Delta m_1$, $\Delta m_2$, …, $\Delta m_m$, …, $\Delta m_n$. Then, the loss mass during the testing period can be obtained:

$$m_m = \Delta m_1 + \Delta m_2 + \cdots + \Delta m_m \tag{1}$$

The relationship between the sample porosity change $\Delta\varphi$ and the corresponding loss mass $\Delta m_m$ is determined as follows:

$$\Delta\varphi = \frac{\Delta m_m}{\pi a^2 h_i \rho_s} \tag{2}$$

where $a$ is the sample radius; $\rho_s$ is the solid particle density; $h_i$ is the real-time sample height caused by particle migration. Assuming that all particles begin to migrate approximately from the bottom, $h_i$ is obtained as

$$h_i = h_0 - \frac{1}{\pi a^2 \rho_s}\left(\Delta m_1 + \Delta m_2 + \cdots + \Delta m_i\right)$$

$$i = 1, 2, \ldots, m \tag{3}$$

Then the porosity at any time can be calculated by

$$\varphi_m = \varphi_0 + \frac{1}{\pi a^2 \rho_s}\left(\Delta m_1 + \Delta m_2 + \cdots + \Delta m_i\right) \tag{4}$$

## 3 Test results and analysis

### 3.1 Constant water pressure loading test

3.1.1 Result of water flow rate variation

Figures 4 (a), 4(b) and 4(c) show the evolution of the water flow rate as a function of time at the constant external water pressures of 0.4, 0.7 and 1.0 MPa. The initial porosities for samples are 0.35, 0.30 and 0.25, respectively.

(1) With the same porosity, the higher the external water pressure, the higher the water flow rate. Under the water pressure of 1.0 MPa, the water flow rate of the filling materials is significantly higher than those under the water pressure of 0.7 MPa and 0.4 MPa, which are 3−5 times and 5−9 times, respectively. It indicates that the external water pressure is the power source of water and mud inrush disasters in the medium of the fault fracture zone.

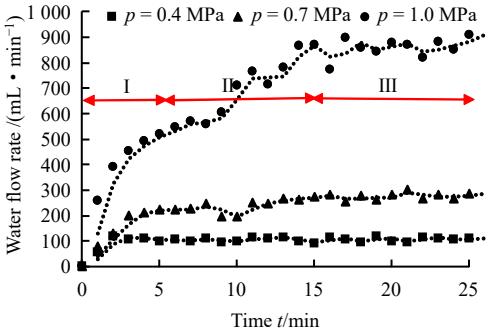


(a) $\varphi_0 = 0.35$

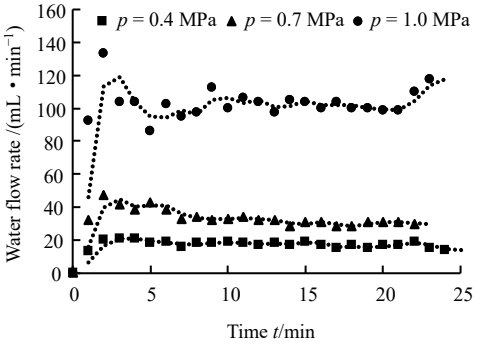


(b) $\varphi_0 = 0.30$

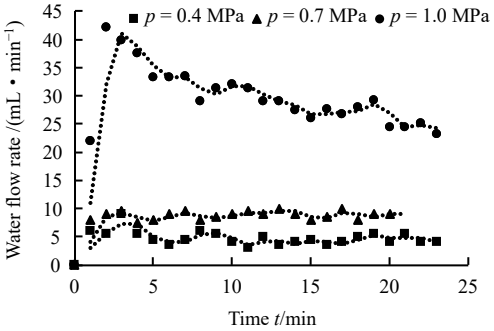


(c) $\varphi_0 = 0.25$

**Fig. 4 Evolution curves of water flow rate**

(2) Under the same water pressure, the greater the initial porosity, the greater the water flow rate. At the pressure of 1 MPa, the maximum water flow rate of the filling materials with the initial porosity of 0.35 is 9 times and 25 times of those for the initial porosity of 0.30 and 0.25, respectively. It reveals that the water and mud inrush disaster will occur in the filling materials of the water-rich fault with a large porosity.

(3) When the initial porosity is 0.35 and the constant water pressure is 1.0 MPa, the muddy water collection during the test is shown in Fig.5. The amount of water inflow gradually increases, and the water quality changes through three stages (clear (I) - turbid (II) - clear (III)). Stage I: The water flow rate increases rapidly. It can be up to 400 mL/min within 3 min and remains stable. Stage II: the water flow rate increases rapidly from 500 mL/min to 900 mL/min under high osmotic pressure. Stage III: the water flow rate stabilizes around 900 mL/min. Compared with the water flow rate curves under other conditions, it can be found that, a sudden increase in the water flow rate is observed at the time of 10 min, the water quality becomes relatively muddy; from this moment on, the water flow rate curve shows a rapid growth, with the maximum water inrush rate up to 905 mL/min.

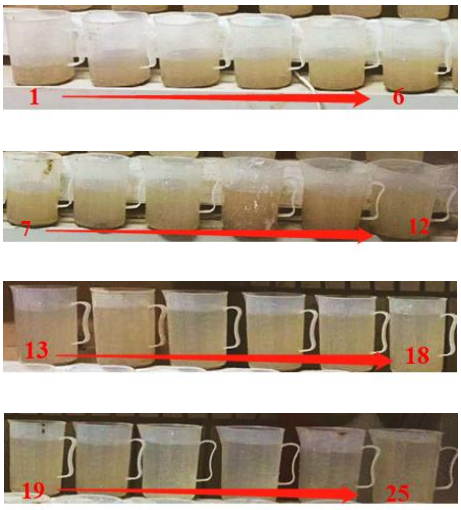


**Fig. 5 Mud collection during the experiment**

3.1.2 Result of particle loss

Figures 6(a), 6(b) and 6(c) show the evolution curves of particle loss over time for samples with initial porosities of 0.35, 0.30 and 0.25 at constant water pressures of 0.4, 0.7 and 1.0 MPa, respectively. It can be seen that:

(1) When the water pressure is low, the loss of particles first increases rapidly and then a slow increase can be witnessed. For high water pressure, the loss of particles increases rapidly in the middle stage of evolution. The loss increases in the early evolution (stage I, 0−3 min) increases rapidly, which is because loose particles in the fracture zone are quickly squeezed and lost under confining pressure at the beginning of the seepage. With an initial porosity of 0.35 and the water pressure of 1 MPa at 10 min, a sharp increase of the particle loss is found (stage II, 3−15 min), lasting 2−3 min. This indicates that under a high water pressure, the pore structure of filling materials gradually increases with the constant migration and outflow of fine particles. Therefore, the loss of coarse particle is induced. As the water flow rate tends to be stable, the water flow channel is formed gradually, and the particle loss decreases gradually (stage III, 15−25 min).

(2) With the same initial porosity, the amount of loss particle increases by time. Additionally, high external water pressure can result in a rapid increase of the particle

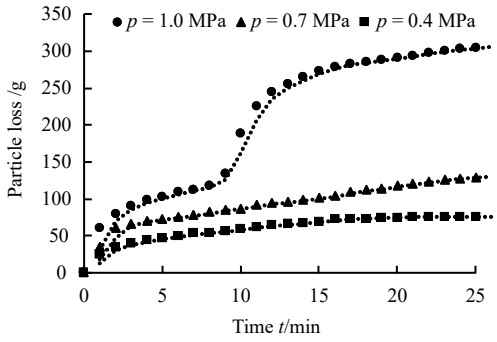


(a) $\varphi_0 = 0.35$

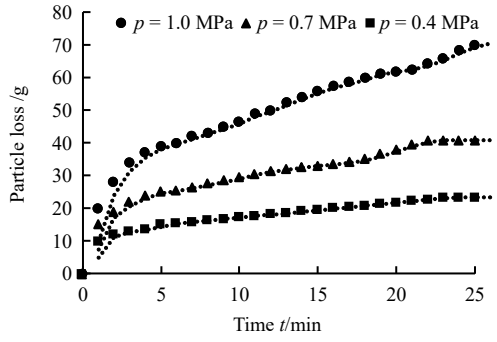


(b) $\varphi_0 = 0.30$

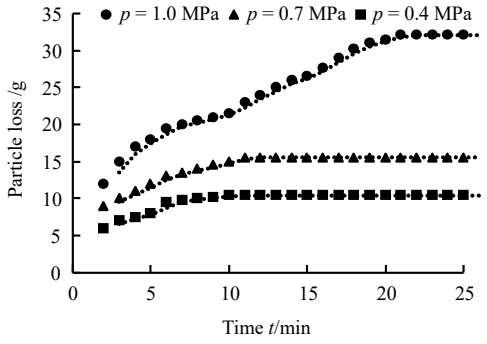


(c) $\varphi_0 = 0.25$

**Fig. 6 Evolution curves of particle loss**

loss. For high external water pressure, the fine particles in the filling materials can be more easily stripped from the skeleton by the water flow and then flow out as moving particles.

(3) Under the same pressure, a large porosity can lead to a sharp increase of the particle loss. It is illustrated there are many movable particles for the loose strata. Therefore, the filling materials will flow out more rapidly under the external hydraulic pressure.

3.1.3 Seepage under different water pressure

(1) Porosity evolution

The porosity is calculated by equation (4), and the porosity evolution curve is shown in Fig.7.

As seen in Fig.7, the evolution of the porosity varies greatly with time with different initial porosities. When the initial porosity is 0.35, the growth rate of porosity is significantly higher than those for the initial porosity of 0.30 and 0.25. Under the same initial porosity condition, the external water pressure is the decisive factor of the porosity evolution. The greater the water pressure is, the more significant the increase of porosity is. Therefore, in practical engineering, the risk of water and mud inrush can be effectively reduced by grouting and other method to increase the stratum strength and reduce the stratum porosity. Moreover, water drainage which can help with pressure relief is also important to reduce the risks.

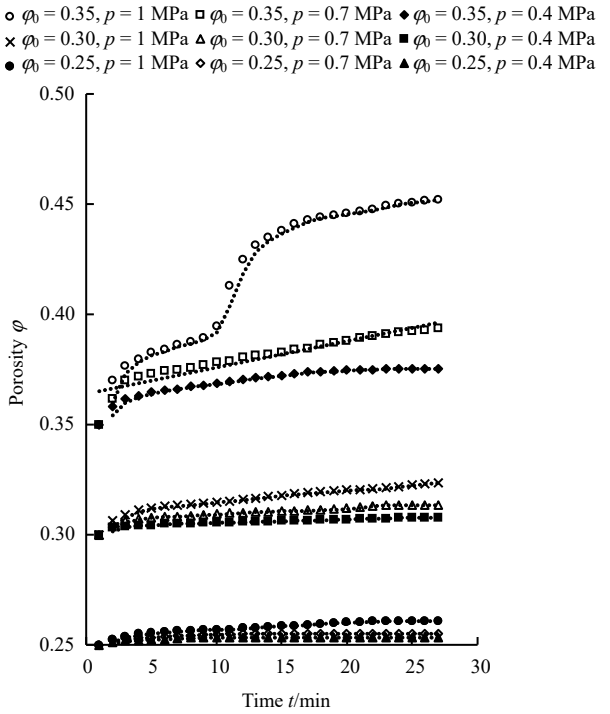


**Fig. 7 Evolution curves of porosity**

(2) Permeability evolution

With the stripping, migration, and loss of fine particles, properties including porosity, permeability and Reynolds number increase accordingly. When the permeability increases to a certain degree, the flow pattern of water will change. In general, the flow state is determined by Reynolds number $Re$[23].

$$Re = \frac{\rho_f v d_p}{\mu\varphi} \tag{5}$$

where $d_p$ is the limiting particle size accounting for 10% of the mass; $v$ is the seepage velocity of water; $\mu$ is the dynamic viscosity of water; $\rho_f$ is the density of water; and $\varphi$ is the porosity of the sample.

The former research results indicate[19] that when the Reynolds number is small ($Re \leqslant 10$), the flow pattern is mainly laminar or transition flow dominated by laminar flow. In this case, the seepage can be determined by Darcy's Law:

$$v = -\frac{k}{\mu}(\nabla p + \rho_f g \nabla z) \tag{6}$$

where $k$ is the permeability of the sample; $\nabla$ is a Hamiltonian operator; $z$ is the direction of gravity; and $g$ is the acceleration due to gravity.

Due to the small size of the sample, the effect of gravity can be ignored, and the seepage flow in the sample can be approximated as one-dimensional seepage flow:

$$v = -\frac{k}{\mu}\frac{\partial p}{\partial z} \tag{7}$$

The seepage velocity can be calculated from the water flow rate $Q$.

$$v = \frac{Q}{\pi a^2} \tag{8}$$

It is assumed that the pressure gradient in the sample is uniformly distributed, then we can obtain as follows:

$$\frac{\partial p}{\partial z} = -\frac{p}{h_i} \tag{9}$$

According to Eqs. (7)−(9), the permeability can be calculated using Eq.(10):

$$k = \frac{Q\mu}{\pi a^2}\frac{h_i}{p} \tag{10}$$

When the Reynolds number is larger than 10 ($Re >$ 10), the seepage is in a turbulent state. In this case, the Forchheimer non-darcy seepage equation[24] can be used

$$-\frac{\partial p}{\partial z} = \frac{\mu}{k}v + \rho_f \beta v^2 \tag{11}$$

where $\beta$ is the non-Darcy seepage inertia coefficient.

Considering the continuous change of seepage with time, then the permeability at the time $t_i$ can be regarded as the average permeability within $t_i - t_{i+1}$. Therefore, the permeability $k_i$ of non-Darcy flow can be obtained by the quadratic polynomial method.

$$k_i = \frac{\mu v_i v_{i+1}(v_{i+1} - v_i)}{(v_{i+1}^2 h_i - v_i^2 h_{i+1})p} h_i h_{i+1},\ i = 1,\ 2,\ \ldots,\ m \tag{12}$$

As seen in Fig.8, the permeability of filling materials

increases with time and the high external pressure can lead to a rapid increase of the permeability. At the initial stage of permeability evolution, the filling materials are extruded rapidly due to confining pressure, inducing a rapid increase of porosity. At the later stage of evolution, the permeability variation trend coincides with the permeability time−varying curve. Under the condition with 1 MPa water pressure and 0.35 initial porosity, the permeability increases from the initial value $5\times10^{-13}$ m$^2$ to $100\times10^{-13}$ m$^2$, which is 20 times increase. In other cases, the increase of the permeability is within the range of 3−8 times.

(3) Reynolds number

When the Reynolds number reaches the critical value, the flow state of water changes from Darcy linear flow to nonlinear flow state.

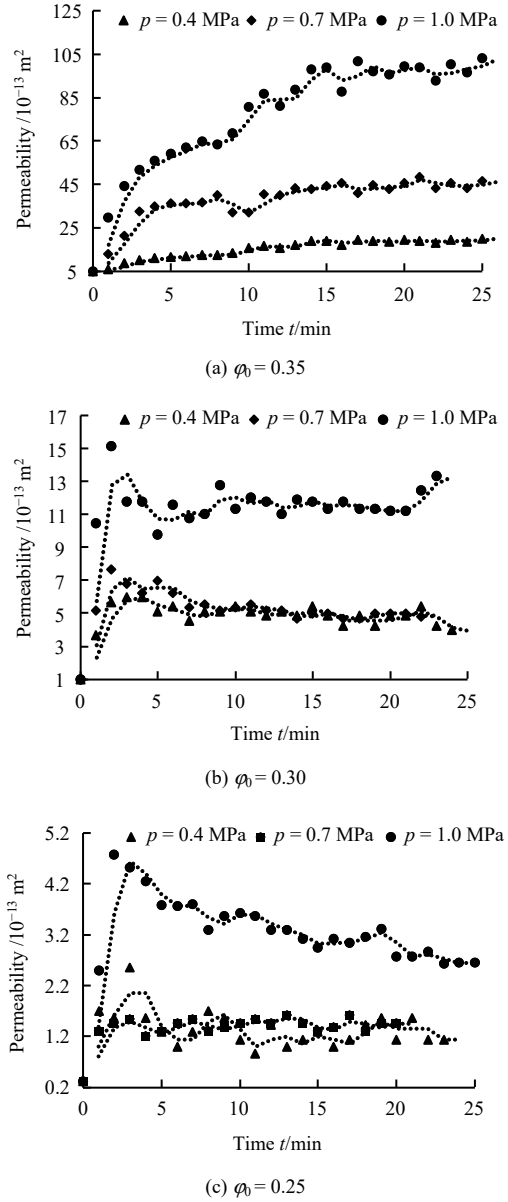


**Fig. 8 Evolution curves of permeability**

Figure 9 shows the Reynolds number increases with time. With the same initial porosity, a high external water pressure results in a fast increase of the Reynolds number. At the initial stage, the porosity of the medium is small and the seepage velocity is low. Therefore, the particle migration is slow. At this stage, the seepage is the linear Darcy flow (Reynolds number below 10). When particles are lost to a certain extent, the porosity and permeability of the formation increase obviously, which leads to the transition of the seepage state from linear Darcy flow to non-Darcy flow. Then the seepage evolution turns into nonlinear flow stage. The Reynolds number increases with the initial porosity at the same external pressure. Under the condition with water pressure of 1 MPa and initial porosity of 0.35 (see Fig.9(a)), the Reynolds number increases from 4.5 to more than 10, indicating that the internal seepage of the medium changes from laminar to turbulent flow at this time and a large amount of movable particles flow out. Therefore, the pores in the filling body are connected and an obvious dominant

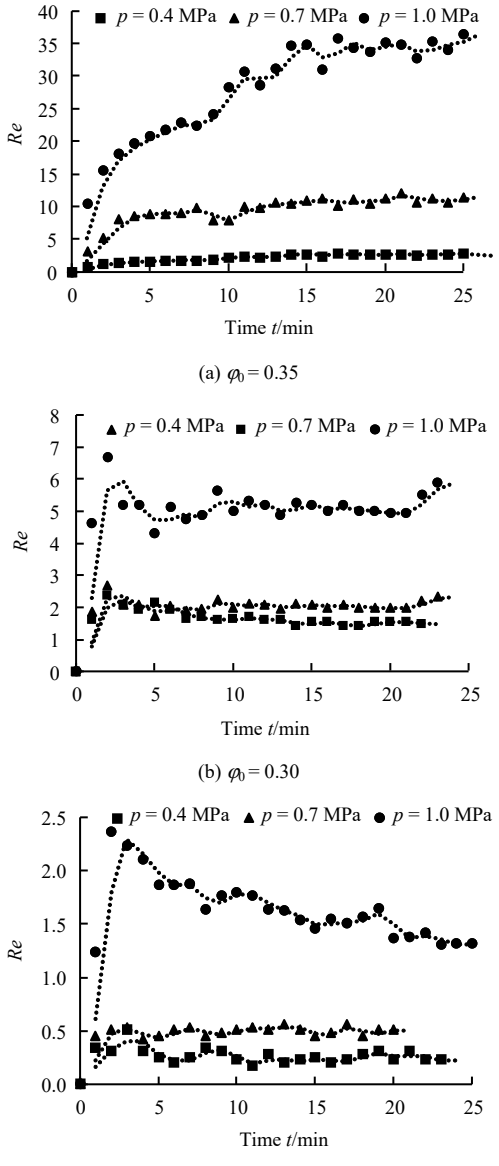


**Fig. 9 Evolution curves of Reynolds number**

seepage channel is formed. As a result, the water flows in pipelines, leading to the direct outflow of water from the channel and the formation of a water inrush disaster.

### 3.2 Gradient hydraulic loading test

The experimental device was used to carry out model tests of water inrush with different hydraulic gradients $i$ and different initial porosities $\varphi$ of the medium, and the test results are shown in Fig.10.

With the increase of hydraulic gradient, water flow rate, particle loss, porosity, *Re*, and permeability increase more rapidly over time. Under the gradient loading condition, the time-varying curve of each variable has a critical point of mutation, and the seepage state of the filling materials can be determined according to the seepage evolution mutation points of parameters such as water flow rate, particle loss and *Re*. Then the critical water pressure of the filling material can be determined.

When the hydraulic gradient is smaller than or equal to 10, the

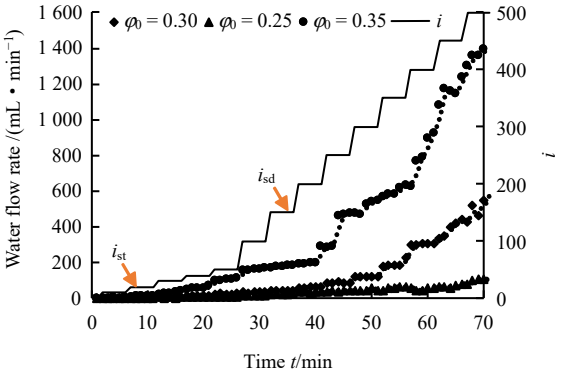


(a) Water flow rate

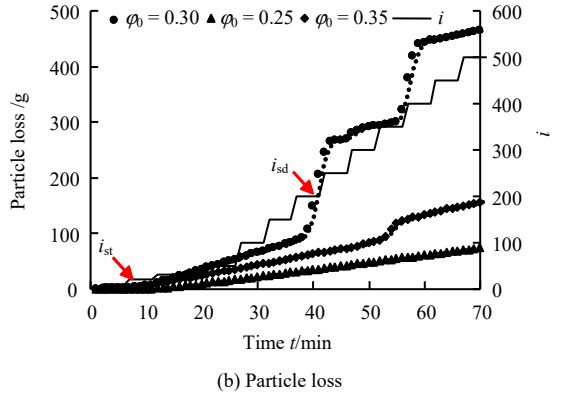


(b) Particle loss

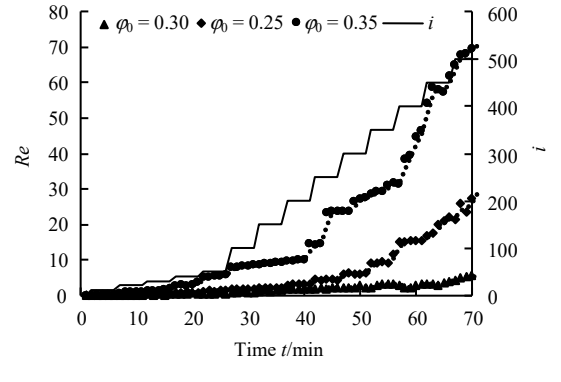


(c) *Re*

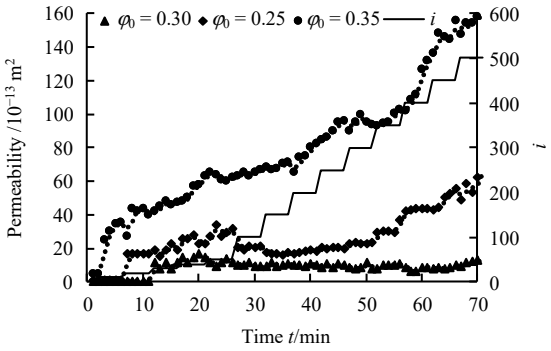


(d) Permeability

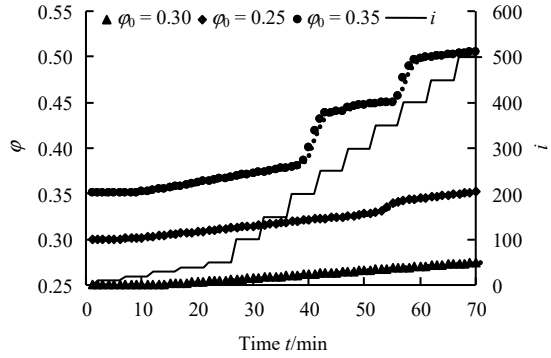


(e) Porosity

**Fig. 10 Time-varying evolution curves of parameters under gradient hydraulic loading**

variation ranges of water flow rate, particle loss (removing particles extruded by confining pressure within the first 3 min) and the variation range of penetration parameter are very limited. Moreover, the Reynolds number is smaller than 10. This indicates that under this hydraulic gradient, there is no hydraulic erosion in filling materials and no start-up of fine particles. The critical hydraulic gradient of particles start-up is called particle starting hydraulic gradient[25−27], which is expressed by $i_{st}$.

When the flow velocity is small, the viscous force is dominant in the seepage flow. As the pressure gradient increases, the water flow rate of filling materials also increases with a small increasing rate. When the pressure gradient reaches a certain value, the flow velocity in the filling materials is relatively large and the inertial force gradually dominates in the seepage flow. Therefore, the time-varying curve of water inflow begins to become excessively nonlinear. This is the critical point where the permeability evolution of the fault fracture zone changes from Darcy flow to non-Darcy flow. With this critical hydraulic gradient, the water flow rate, particle loss, permeability, porosity and *Re* of the filling materials begin to increase rapidly. The results show that the particle flow in the fracture zone is rapidly eroded and stripped away, and the seepage changes from laminar flow to turbulent flow with this hydraulic gradient. At this time, the critical hydraulic gradient is called the hydraulic gradient of flow state transition, which is ex-

pressed by $i_{sd}$. Different initial porosities correspond to different $i_{sd}$. The larger the initial porosity is, the smaller $i_{sd}$ is.

Therefore, the critical water pressure of particle starting can be determined according to the evolution curve of particle loss under gradient hydraulic loading. Based on the evolution curve of water flow rate under gradient hydraulic loading, the critical water pressure for the transition of seepage flow pattern in fault fracture zones can be determined. Thus the critical point of the evolution of water and mud inrush in the fault fracture zone can be determined.

### 3.3 Tests under two hydraulic loading modes

Table 2 shows that the maximum water flow rate, particle loss, permeability, *Re* and porosity under gradient hydraulic loading conditions are obviously greater than those under constant water pressure conditions. With the water pressures of 0.4, 0.7 and 1.0 MPa, the maximum water flow rates under three gradient hydraulic loadings are 1.8, 2.2 and 1.6 times of those under constant water pressure, respectively. The maximum particle loss masses under gradient hydraulic loadings are 1.2, 2.1 and 1.5 times of those under constant water pressure.

**Table 2 Comparison of variables under two hydraulic loading conditions**

| *p*/MPa | Loading | Water flow rate /(mL • min$^{-1}$) | Particle loss/g | Permeability/$10^{-13}$ m$^2$ | *Re* | Porosity | | |
|---|---|---|---|---|---|---|---|---|
| | | | | | | $\varphi_0 = 0.35$ | $\varphi_0 = 0.30$ | $\varphi_0 = 0.25$ |
| 0.4 | Constant | 110 | 76 | 20 | 2.6 | 0.375 | 0.308 | 0.253 |
| | Gradient | 201 | 90 | 75 | 10.0 | 0.386 | 0.320 | 0.261 |
| 0.7 | Constant | 286 | 131 | 40 | 15.0 | 0.394 | 0.314 | 0.255 |
| | Gradient | 635 | 278 | 100 | 31.0 | 0.449 | 0.341 | 0.268 |
| 1.0 | Constant | 905 | 307 | 100 | 36.0 | 0.452 | 0.324 | 0.261 |
| | Gradient | 1 426 | 467 | 161 | 71.0 | 0.506 | 0.353 | 0.276 |

The maximum permeabilities with gradient hydraulic loadings are 3.8, 2.5 and 1.6 times of those under constant hydraulic loading, and the maximum Reynolds numbers under gradient hydraulic loadings are 3.8, 2.1 and 2.0 times of those with constant hydraulic loading. With the initial porosity of 0.35 and the water pressures of 1.0, 0.7 and 0.4 MPa, the maximum porosities under gradient water pressure loadings are increased by 11.9%, 14.0% and 2.9%, respectively compared with those under constant water pressure. With the initial porosity of 0.30 and the water pressures of 1.0, 0.7 and 0.4 MPa, the maximum porosities under gradient water pressure loadings are increased by 9.0%, 8.6% and 3.9%, respectively compared with those under constant water pressure. For the initial porosity of 0.25 and the water pressures of 1.0, 0.7 and 0.4 MPa, the maximum porosities under gradient hydraulic loadings are increased by 5.7%, 5.1% and 3.2%, respectively compared with that under constant water pressure.

By comparing the experimental results of the two loading modes, it is found that under the gradient loading mode, the evolution characteristics of the medium in the fault fracture zone are more obvious than that under the condition of constant hydraulic loading. The critical pressure of water and mud inrush is smaller. Under the gradient loading, the water flow rate, particle loss and permeability parameters increase significantly compared with that with the constant loading. This indicates that the excavation leads to the gradual increase of hydraulic gradient in the water-resistant structure, which further aggravates the risk of water and mud inrush. When the permeability evolution in the water-resistant structure changes from laminar to turbulent flow, the water pressure under gradient hydraulic loading is significantly lower than that under the constant hydraulic pressure. This reveals that the increase in the hydraulic gradient in the water-resistant structure caused by excavation weakens the ability of blocking water and mud of the water-resistant structure. Therefore, the critical water pressure of the water and mud inrush of the water-resistant structure under the traditional constant water pressure is smaller than the critical water pressure value from actual fault.

## 4 Characteristics of permeability evolution in fault fracture zones under high osmotic pressure

### 4.1 Analysis of flow state transformation based on *Q*–*t* and *i*–*Q* relationships

Under the action of high osmotic pressure, the permeability of fault fracture zones changes with water pressure. The water pressure is an important parameter for water inrush in tunnel through the fault fracture zone. Under high water pressure, the aquifer structure has a great potential energy of motion, which can accelerate the process of water and mud inrush in the fault fracture zones.

Based on the analysis of the test data of water flow rate, the flow pattern transformation rule of the filling materials under the action of high osmotic pressure is revealed.

4.1.1 Analysis of flow state transformation based on *Q*–*t* relationship

The *Q*–*t* relationship (Fig.11) can directly show the evolution process of water and mud inrush in fault

fracture zones. Therefore, flow pattern transformation analysis based on $Q$−$t$ relationship is helpful to understand the process of water and mud inrush in water-rich fault fracture zones.

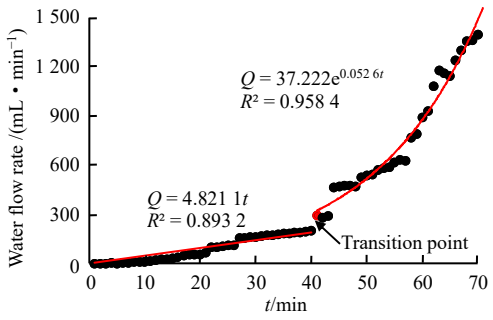


**Fig. 11 Relationship between $Q$ and $t$**

The $Q$−$t$ relationship curve has obvious segmentation characteristics and two mainly segments can be identified as follows:

Stage I: laminar flow phase, namely the Darcy flow phase. The seepage mainly occurs at the early stage of the high-pressure seepage evolution test. The water flow rate increases continuously with pressure, and there is an obvious linear relationship between the water flow rate and time at this stage. The $Q$−$t$ curve is a straight line through the origin, and the relationship can be expressed as follows:

$$Q=\alpha t\left(0<i<i_{\mathrm{sd}}\right) \tag{13}$$

where $\alpha$ is the proportion coefficient and $i_{\mathrm{sd}}$ is the critical hydraulic gradient.

Stage II: turbulent flow phase, namely non-Darcy flow phase. The seepage mainly occurs at the late stage of the high-pressure seepage evolution test. The water flow rate increases rapidly with the pressure. At this stage, the water flow rate has an obvious nonlinear relationship with the time. The $Q$−$t$ curve tends to be an exponential curve, and the relationship can be expressed as follows:

$$Q=\beta \mathrm{e}^{\gamma t}\left(i_{\mathrm{sd}}\leqslant i\right) \tag{14}$$

Where $\beta$ and $\gamma$ are the proportional coefficients; and $i_{\mathrm{sd}}$ is the critical hydraulic gradient.

The transition point ($Q_{\mathrm{sd}}$, $i_{\mathrm{sd}}$) is an important characteristic point. The relationship is linear before the transition point ($Q_{\mathrm{sd}}$, $i_{\mathrm{sd}}$) and the relationship is nonlinear after the transition point ($Q_{\mathrm{sd}}$, $i_{\mathrm{sd}}$). For $0<i<i_{\mathrm{sd}}$, the seepage in the fault fracture zone is Darcy flow. At this time, the permeability of the fault fracture zone is small and the water resistance ability is strong. For $i_{\mathrm{sd}}\leqslant i$, the particles quickly migrate, and the seepage changes to non-Darcy flow. Then seepage channels are gradually formed. The permeability in the fracture zone increases, and the water resistance ability decreases.

Therefore, the mathematical model of flow pattern transformation of seepage flow in fault fracture zones under high osmotic pressure can be expressed as follows:

$$Q=\begin{cases}\alpha t\left(0<i<i_{\mathrm{sd}}\right)\\ \beta \mathrm{e}^{\gamma t}\left(i_{\mathrm{sd}}\leqslant i\right)\end{cases} \tag{15}$$

4.1.2 Analysis of flow state transformation based on the $i$−$Q$ relation

The $i$−$Q$ relationship (Fig.12) can reflect the critical hydraulic gradient in the evolution process of water and mud inrush in the fault fracture zones. Therefore, the analysis of flow pattern transformation based on $i$−$Q$ relationship is helpful to deeply understand the controlling role of high osmotic pressure on the evolution of water and mud inrush in the water-rich fault fracture zones.

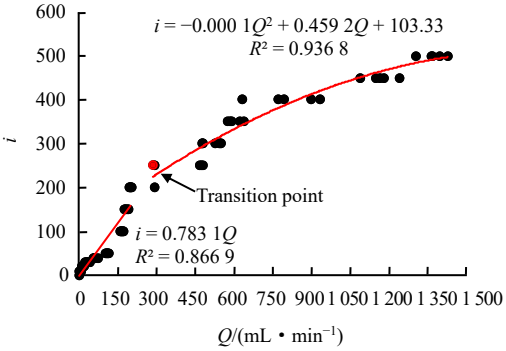


**Fig. 12 Relationship between $i$ and $Q$**

As can be seen from Fig.12, The $i$−$Q$ relationship curve has obvious segmentation characteristics and two mainly segments can be identified as follows:

Stage I: laminar flow phase, namely the Darcy flow phase. The seepage mainly occurs at the early stage of the high-pressure seepage evolution test and the water flow rate increases with the pressure. At this stage, the water flow rate has an obvious linear relationship with the time. The $i$−$Q$ curve is a straight line through the origin, and the relationship can be expressed as follows:

$$i=\delta Q\left(0<i<i_{\mathrm{sd}}\right) \tag{16}$$

Where $\delta$ is the proportionality coefficient.

Stage II: turbulent flow phase, namely non-Darcy flow phase. The seepage mainly occurs at the late stage of the high-pressure seepage evolution test. The water flow rate increases rapidly with the pressure. During this stage, the water flow rate and the hydraulic gradient have an obvious nonlinear relationship, and the relationship can be expressed as follows:

$$i=\varepsilon\left(Q-Q_{\mathrm{sd}}\right)^{\eta}+i_{\mathrm{sd}}\left(i_{\mathrm{sd}}\leqslant i\right) \tag{17}$$

Where $\varepsilon$ and $\eta$ are the proportional coefficients; $Q_{\mathrm{sd}}$ is the water flow rate at the transition point.

The transition point ($Q_{\mathrm{sd}}$, $i_{\mathrm{sd}}$) is an important characteristic point. The relationship is linear before the transition point ($Q_{\mathrm{sd}}$, $i_{\mathrm{sd}}$) and the relationship is nonlinear after the transition point ($Q_{\mathrm{sd}}$, $i_{\mathrm{sd}}$). For $0<i<i_{\mathrm{sd}}$, the seepage turns to Darcy flow. The permeability in the fracture zone is small and the water resistance ability is strong.

For $i_{sd} \leqslant i$, the particles quickly migrate and the seepage changes to non-Darcy flow. Then seepage channels are gradually formed. The permeability in the fracture zone increases, and the water resistance ability decreases.

Therefore, the mathematical model of flow pattern transformation of seepage flow in fault fracture zones under high osmotic pressure can be expressed as follows:

$$i = \begin{cases} \delta Q \left(0 < i < i_{sd}\right) \\ \varepsilon \left(Q - Q_{sd}\right)^{\eta} + i_{sd} \left(i_{sd} \leqslant i\right) \end{cases} \tag{18}$$

### 4.2 Characteristics of permeability evolution of fault fracture zones under high osmotic pressure

The parameter permeability can represent the permeability resistance of the fault fracture zone. The permeability data in tests are analyzed, and the permeability evolution characteristics of the fracture zone under the action of high osmotic pressure are further revealed.

As seen in Fig.13, the $k$–$i$ relationship curve has obvious segmentation characteristics and can be mainly divided into the following three sections:

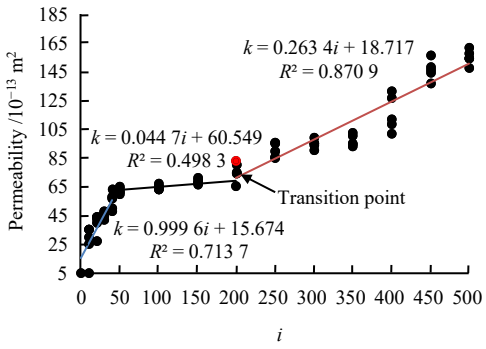


**Fig. 13 Relationship between of $k$ and $i$**

Stage I: a phase in which the permeability of the fault fracture zones increases under the action of confining pressure. The permeability at this stage increases rapidly during a short period. As the tunnel is excavated, a free face is formed. The loose particles in the fault fracture zone are quickly squeezed and flow away under confining pressure, which leads to an rapid increase in permeability of the filling materials in a short time. The permeability of the fracture zone increases linearly with water pressure:

$$k_{I} = a_{I} i + k_{0} \left(0 < i < i_{st}\right) \tag{19}$$

Stage II: a phase in which initial impermeability is witnessed in the fractured zones under low pressure. The permeability increases slowly with time, and the $k$–$i$ curve is approximately in parallel with the horizontal $X$-axis. The relationship between $k$ and $i$ can be expressed as follows:

$$k_{II} = a_{II} i + b_{II} \left(i_{st} < i < i_{sd}\right) \tag{20}$$

Stage III: a phase in which an abrupt change of permeability of fracture zone is found under high water pressure. At this stage, the permeability of the fracture zone changes significantly under the action of high pressure. Additionally, the permeability of fracture zone increases linearly with the pressure and the flow state of the fractured zone changes from laminar to turbulent. The relationship between $k$ and $i$ can be expressed as follows:

$$k_{III} = a_{III} i + b_{III} \left(i_{sd} < i\right) \tag{21}$$

Based on the above analysis, a generalized model of permeability evolution under high osmotic pressure in fault fracture zones is proposed. The two points ($k_{I}$, $i_{st}$) and ($k_{II}$, $i_{sd}$) are important. The permeability evolution process of the fault fracture zone under high osmotic pressure can be divided into the stage in which the permeability of the fracture zone increases under confining pressure, the stage in which the initial impermeability of the fracture zone is witnessed under low pressure and the stage in which an abrupt change of the permeability of the fracture zone is detected under high pressure. Therefore, a generalized model for descryptions of permeability characteristics in the fractured zone under high osmotic pressure can be expressed as follows:

$$\left.\begin{aligned} k_{I} &= a_{I} i + k_{0} \left(0 < i < i_{st}\right) \\ k_{II} &= a_{II} i + b_{II} \left(i_{st} < i < i_{sd}\right) \\ k_{III} &= a_{III} i + b_{III} \left(i_{sd} < i\right) \end{aligned}\right\} \tag{22}$$

## 5 Conclusions

A large-scale indoor water and mud inrush test system considering mass transfer and crustal stress state is designed. The three influencing factors for tunnel excavation including high osmotic pressure, excavation disturbance and permeability resistance of medium are investigated. Meanwhile, the evolution mechanism of water and mud inrush disasters in the water-rich fault fractured tunnel is simulated with constant pressure loading, gradient pressure loading, and different initial porosities of the medium. The main conclusions of the experiment are shown as follows:

(1) Evolution of water and mud inrush disasters in fault fractured zones is a strong coupling process of seepage and erosion. In the beginning, fine particles in the filling of fracture zones migrate under the water pressure. Then, with the continuous migration and loss of fine particles, the flow pattern changes from laminar flow to turbulent flow, which eventually leads to water and mud inrush disasters.

(2) With the higher osmotic pressure and the larger initial porosity of the filling in fractured zone, the parameters including the water flow rate, the particle loss mass and the permeability will increase more rapidly and the evolution characteristics of water and mud inrush

are more obvious in the test.

(3) The evolution characteristics of water and mud inrush are more obvious under the gradient loading than under the constant water pressure loading. With the critical water pressure, the flow pattern in the fillings will change.

(4) A generalized model for the description of permeability evolution characteristics of faults is constructed by analyzing flow state transition based on the relationships between water flow rate and time ($Q-t$), hydraulic gradient and water flow rate ($i-Q$). Moreover, the relationship between permeability and hydraulic gradient ($k-i$) to describe the evolution characteristics of permeability is considered in this generalized model.

## References

[1] QIAN Qi-hu. Challenges faced by underground projects Construction safety and countermeasures[J]. Chinese Journal of Rock Mechanics and Engineering, 2012, 31(10): 1945−1956.

[2] LI Shu-cai, XU Zhen-hao, HUANG Xin, et al. Classification, geological identification, hazard mode and typical case studies of hazard-causing structures for water and mud inrush in tunnels[J]. Chinese Journal of Rock Mechanics and Engineering, 2018, 37(5): 1043−1069.

[3] LUO Xiong-wen. Study on disastrous structures and models of water-burst and mud-burst in deep and long tunnel[D]. Beijing: China Academy of Railway Sciences, 2014.

[4] XU Da-cheng. Construction technology of mud inrush in fracture zone in Yanmenguan tunnel[J]. Railway Engineering, 2014(11): 72−74.

[5] WEN Wen-zhao. Construction technology in high pressure and water-rich section of the fault in Beitianshan tunnel Jinghe-Yili-Huoerguosi railway[J]. Railway Standard Design, 2009(6): 90−92.

[6] LI Sheng-jie, XIE Yong-li, ZHU Xiao-ming. Research on countermeasure of water gushing with collapse in process of Wushaoling highway tunnel crossing F4 fault fracture zone[J]. Chinese Journal of Rock Mechanics and Engineering, 2013, 32(Suppl.2): 3602−3609.

[7] ZHANG Min-qing, HUANG Hong-jian, YIN Huai-lian, et al. Water outburst treatment at fault F3 in Bieyancao tunnel on Yiwan railway[J]. Modern Tunnelling Technology, 2006, 43(2): 67−69.

[8] ZHANG Hui-ling, FAN Sheng-ming. Researchon the treatment of tunnel mud bursting at a fault zone[J]. Modern Tunnelling Technology, 2017, 54(1): 186−190.

[9] ZHANG Zhi-qiang, HE Ben-guo, WANG Zhi-jie, et al. Study of method and effect of high-position drainage of tunnel in water-rich fault[J]. Rock and Soil Mechanics, 2012, 33(11): 3359−3366.

[10] LI Sen-sen. The technical research of geological hazards treatment on water and mud burst in Lingjiao tunnel fault fracture zone[D]. Xi′an: Chang′an University, 2013.

[11] LI Xiao-zhao, LUO Guo-yu, CHEN Zhong-sheng. The mechanism of deformation and water conduction of fault due to excavation in water inrush in underground engineering[J]. Chinese Journal of Geotechnical Engineering, 2002, 24(6): 695−700.

[12] WU Qiang, LIU Jin-tao, ZHONG Ya-ping, et al. The numerical simulations of water-bursting time-effect for faults in Zhaogezhuang Coal Mine, Kailuan, China[J]. Journal of China Coal Society, 2002, 27(5): 511−516.

[13] SHI L Q, SINGH R N. Study of mine water inrush from floor strata through faults[J]. Mine Water and the Enviroment, 2001, 20(3): 140−147.

[14] JEON S, KIM J, SEO Y, et al. Effect of a fault and weak plane on the stability of a tunnel in rock—a scaled model test and numerical analysis[J]. International Journal of Rock Mechanics and Mining Sciences, 2004, 41(3): 486−491.

[15] MA D, REZANIA M, YU H S, et al. Variation of hydraulic properties of granular sandstones during water inrush: effect of small particle migration[J]. Engineering Geology, 2017, 217: 61−70.

[16] LI Li-ping, LIU Shang, LI Shu-cai, et al. Development of testing system for coupled seepage and triaxial stress measurements and its application to permeability characteristic test on filling medium[J]. Rock and Soil Mechanics, 2017, 38(10): 3053−3061.

[17] LI Ting-chun, LÜ Lian, DUAN Hui-ling, et al. Water burst mechanism of deep buried tunnel passing through weak water-rich zone[J]. Journal of Central South University (Science and Technology), 2016, 47(10): 3469−3476.

[18] YAO Bang-hua. Theory and application of fluid-solid coupling dynamics with variable mass for fractured rock mass[D]. Xuzhou: China University of Mining and Technology, 2012.

[19] WANG Lu-zhen, CHEN Zhan-qing, KONG Hai-ling, et al. Experimental study of impact of loading history on permeability characteristics of broken coal with different grain size gradations[J]. Rock and Soil Mechanics, 2013, 34(5): 1325−1330.

[20] ZHANG Rui. Activated seepage conduction mechanism of floor tectonic fracture zone in mining under pressure[D]. Xuzhou: China University of Mining and Technology, 2014.

[21] CHANG D S, ZHANG L M. Critical hydraulic gradients of internal erosion under complex stress states[J]. Journal of Geotechnical and Geoenvironmental Engineering, 2013, 139(9): 1454−1467.

[22] LIU J Q, CHEN W Z, LIU T G, et al. Effects of initial porosity and water pressure on seepage-erosion properties of water inrush in completely weathered granite[J]. Geofluids, 2018: 1-11. DOI: 10.1155/2018/4103645.

[23] OERTEL H J, BÖHLE M, MAYES K, et al. Prandtl's essentials of fluid mechanics[M]. New York: Springer, 2009.

[24] WHITAKER S. The forchheimer equation: a theorerical development[J]. Transport in Porous Media, 1996, 25(1): 27−61.

[25] HAGHIGHI I, CHEVALIER C, DUC M, et al. Improvement of hole erosion test and results on reference soils[J]. Journal of Geotechnical and Geoenvironmental Engineering, 2013, 139(2): 330−339.

[26] BENDAHMANE F, MAROT D, ALEXIS A. Experimental parametric study of suffusion and backward erosion[J]. Journal of Geotechnical and Geoenvironmental Engineering, 2008, 134(1): 57−67.

[27] CHANEY R C, DEMARS K R, REDDI L N, et al. Comparison of internal and surface erosion using flow pump tests on a sand-kaolinite mixture[J]. Geotechnical Testing Journal, 2000, 23(1): 116−122.